Chemical Science

Accepted Manuscript

This article can be cited before page numbers have been issued, to do this please use: J. Wang, J. H. Marks, C. Zhang, A. M. Turner, M. McAnally, M. Nogamida and R. I. Kaiser, *Chem. Sci.*, 2026, DOI: 10.1039/D6SC04215E.

ROYAL SOCIETY OF CHEMISTRY

rsc.li/chemical-science

View Article Online
DOI: 10.1039/D6SC04215E

Non-Equilibrium Formation of the Elusive Dibridged Diboranyl (B_2H_5) Radical and Boranes in Low-Temperature Diborane Ices

Jia Wang,[1,2] Joshua H. Marks,[1,2] Chaojiang Zhang,[1,2] Andrew M. Turner,[1,2] Mason McAnally,[1,2] Miori Nogamida,[1,2,3] Ralf I. Kaiser[1,2*]

[1] *W. M. Keck Research Laboratory in Astrochemistry, University of Hawaii at Manoa, Honolulu, HI 96822, United States*

[2] *Department of Chemistry, University of Hawaii at Manoa, Honolulu, HI 96822, United States*

[3] *Present address: Chuo University, 1-13-27 Kasuga, Bunkyo-ku, Tokyo 112-8551, Japan*

[*]Corresponding Author:
Ralf I. Kaiser, ralfk@hawaii.edu

Abstract

Boranes are prototypical electron-deficient species central to the boron chemistry and chemical vapor deposition. Despite extensive studies of diborane (B_2H_6), key reactive intermediates—particularly the monobridged and dibridged diboranyl (B_2H_5) radicals—have remained incompletely characterized because of their high reactivity. Here, we report the experimental identification of the hitherto elusive dibridged diboranyl radical together with its monobridged isomer in low-temperature diborane ices exposed to energetic electron irradiation. The radicals were identified in irradiated diborane and fully deuterated diborane-d_6 ices at 40 K via Fourier transform infrared spectroscopy, revealing the formation of the monobridged radical through B–H bond cleavage, followed by isomerization to the dibridged isomer. Additionally, utilizing vacuum ultraviolet photoionization reflectron time-of-flight mass spectrometry combined with isotopic labeling experiments, complex boranes ranging from B_6H_{10} to $B_{12}H_{26}$ were detected in the gas phase during temperature-programmed desorption. The formation of these increasingly complex boranes is proposed to proceed through sequential boron-insertion reactions involving BH and BH_3 addition coupled with hydrogenation pathways. These findings highlight the critical role of non-equilibrium chemistry in the synthesis of reactive diboranyl radicals and complex

View Article Online
DOI: 10.1039/D6SC04215E

boranes in low-temperature ices, providing fundamental insight into boron chemistry under extreme conditions.

Introduction

Since the pioneering identification of boranes (B_4H_{10}) by Stock more than a century ago (1912),[1] boranes (boron hydrides) have attracted sustained interest across the inorganic chemistry,[2-5] physical chemistry,[6-9] and computational chemistry communities.[10-12] This interest arises largely from the critical roles of boranes as prototypical systems for understanding electron-deficient bonding.[12-14] Based on the three-center B–H–B bridging bond framework formulated by Longuet-Higgins,[15] Lipscomb deduced the nature of chemical bonding in boranes, providing fundamental insights into chemical bonding theory and motivating the development of topological approaches to molecular structure.[16,17] Beyond their fundamental importance, the thermal or electron-induced decomposition of diborane (B_2H_6, **1**) generates reactive intermediates, providing direct insight into B–H bond cleavage, radical isomerization, and molecular mass growth pathways toward larger boranes.[13,18] Moreover, atomic boron has been detected in diffuse interstellar clouds with a gas-phase abundance of around 2.5×10^{-10} relative to atomic hydrogen,[19,20] representing a depletion of approximately 60% relative to the meteoritic boron abundance of $(6.0 \pm 0.6) \times 10^{-10}$,[20,21] suggesting the potential formation of boron-bearing species on dust grains under astrophysical conditions. Despite extensive investigations of boranes such as diborane,[22,23] key reactive intermediates—particularly the monobridged (C_{2v}, **2**) and dibridged (C_s, **3**) diboranyl (B_2H_5) radicals—remain incompletely characterized due to their high reactivity.

Diborane is the smallest stable borane and a benchmark system featuring three-center two-electron (3c-2e) bonding.[3,8] This distinctive bonding framework underpins its intrinsic stability and governs its complex reactivity, particularly under energetic or dissociative conditions. Diborane can undergo B–H bond cleavage to form the monobridged (**2**) and dibridged (**3**) diboranyl radicals, with the monobridged isomer being approximately 20 kJ mol^{-1} more stable than its dibridged counterpart (**3**).[10,11] These radicals serve as key intermediates in the formation of more complex boranes. The monobridged diboranyl radical (**2**) was first identified by photoionization mass spectrometry via reaction of diborane with fluorine atoms,[6] and later characterized by infrared spectroscopy in low-temperature (10 K) diborane ices subjected to irradiation by energetic electrons.[13] In contrast, although the dibridged diboranyl radical (**3**) has

View Article Online
DOI: 10.1039/D6SC04215E

been tentatively detected via photoionization mass spectrometry,[6] its direct identification remains elusive. Unambiguous identification of this dibridged isomer under controlled conditions is therefore essential for elucidating fundamental reaction pathways in boron chemistry, including hydrogen abstraction, radical isomerization, and molecular mass growth leading to complex boranes, as well as processes relevant to chemical vapor deposition and astrochemistry.

Here, we report the formation of monobridged (**2**) and dibridged (**3**) diboranyl radicals in low-temperature diborane (**1**) ices, with the dibridged isomer experimentally identified for the first time. Diborane (B_2H_6) and fully deuterated diborane-d_6 (B_2D_6) ices were prepared in separate experiments with thicknesses of 510 ± 50 nm at 5 K and subsequently exposed to energetic electrons at 40 K, thereby initiating bond cleavage through ionizing radiation, followed by their detection via Fourier transform infrared (FTIR) spectroscopy (Supplementary information). After irradiation, the ices were heated from 40 to 320 K at a rate of 1 K min^{-1} under temperature-programmed desorption (TPD) conditions. Utilizing vacuum ultraviolet (VUV) photoionization reflectron time-of-flight mass spectrometry (PI-ReToF-MS), boranes ranging from B_6H_{10} to $B_{12}H_{26}$ were detected in the gas phase during TPD of the irradiated ices. Among these, B_9H_{19}, $B_{10}H_{22}$, $B_{11}H_{19}$, $B_{12}H_{22}$, and $B_{12}H_{26}$ are, to the best of our knowledge, identified for the first time. These findings reveal non-equilibrium pathways towards the synthesis of monobridged (**2**) and dibridged (**3**) diboranyl radicals along with complex boranes in low-temperature diborane ices, providing fundamental insight into boron chemistry in extreme environments.

Results

Infrared spectroscopy

Fourier transform infrared (FTIR) spectroscopy was employed to monitor diborane (B_2H_6) and fully deuterated diborane-d_6 (B_2D_6) ices before, during, and after irradiation at 40 K (Figs. 1–4, Figs. S1–S2). Detailed assignments of the FTIR spectra are compiled in Tables S1–S2. Diborane (10% in hydrogen) or diborane-d_6 (10% in deuterium) were deposited onto the cold substrate at 5 K. After deposition, the ices were heated to 40 K to remove the hydrogen or deuterium gas from the ices. Prior to irradiation, the observed absorptions arise from the fundamentals and combination modes of the diboranes; prominent features in unprocessed B_2H_6 ice include the BH_2 asymmetric

View Article Online
DOI: 10.1039/D6SC04215E

stretching mode (ν_8) at 2600 cm^{-1}, the ring deformation mode (ν_{17}) at 1578 cm^{-1}, and the BH_2 scissoring mode (ν_3) at 1163 cm^{-1}.[24] Following irradiation, new absorption features emerge in

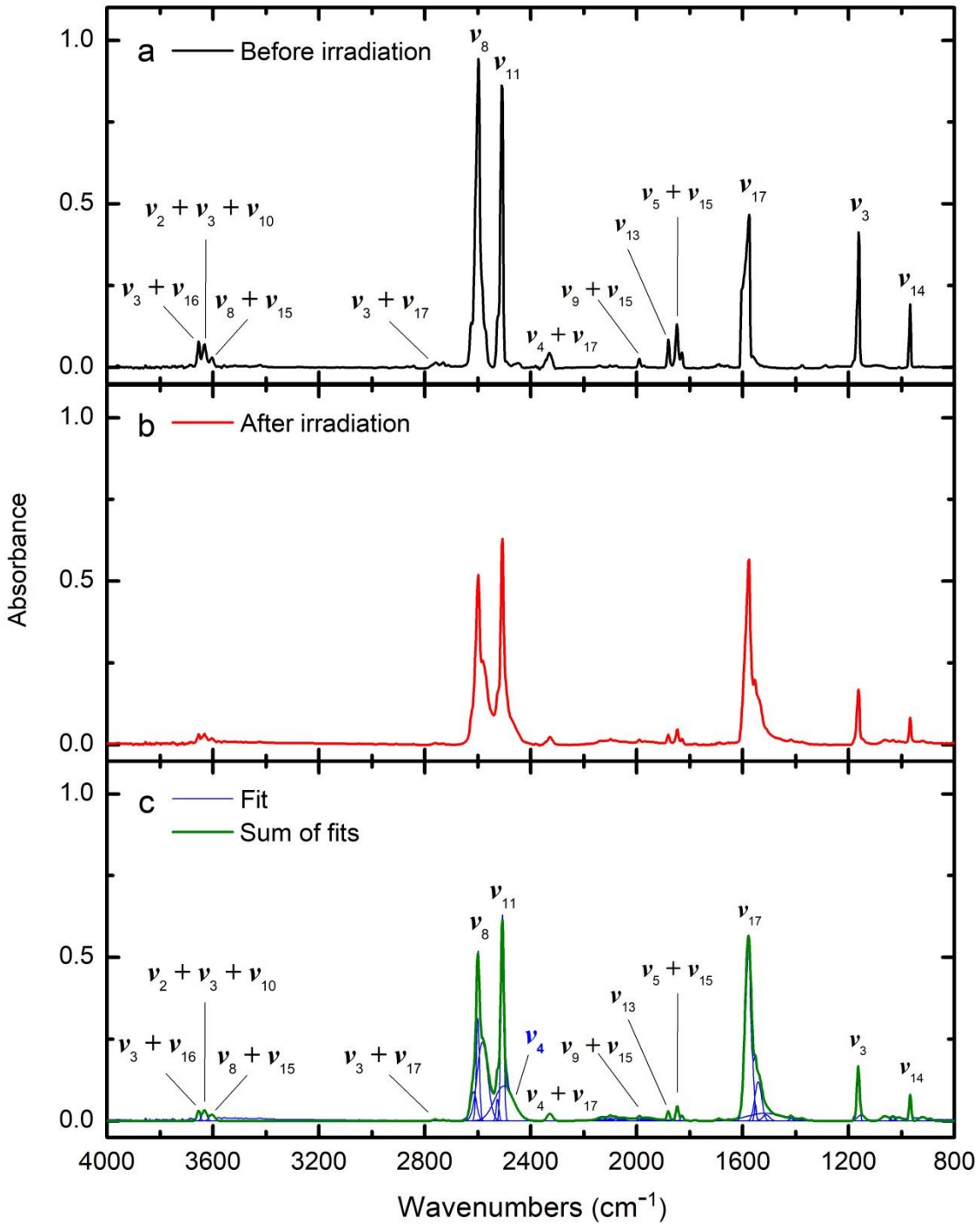

Fig. 1 FTIR spectra of diborane (B_2H_6) ice at 40 K before (a) and after (b) irradiation at a current of 125 nA for 120 minutes (a). The green trace represents the sum of the individual fitted

View Article Online
DOI: 10.1039/D6SC04215E

components of the infrared spectrum after irradiation (c). Detailed assignments are compiled in Table S1. The mono diboranyl (B_2H_5) radical was labeled in blue.

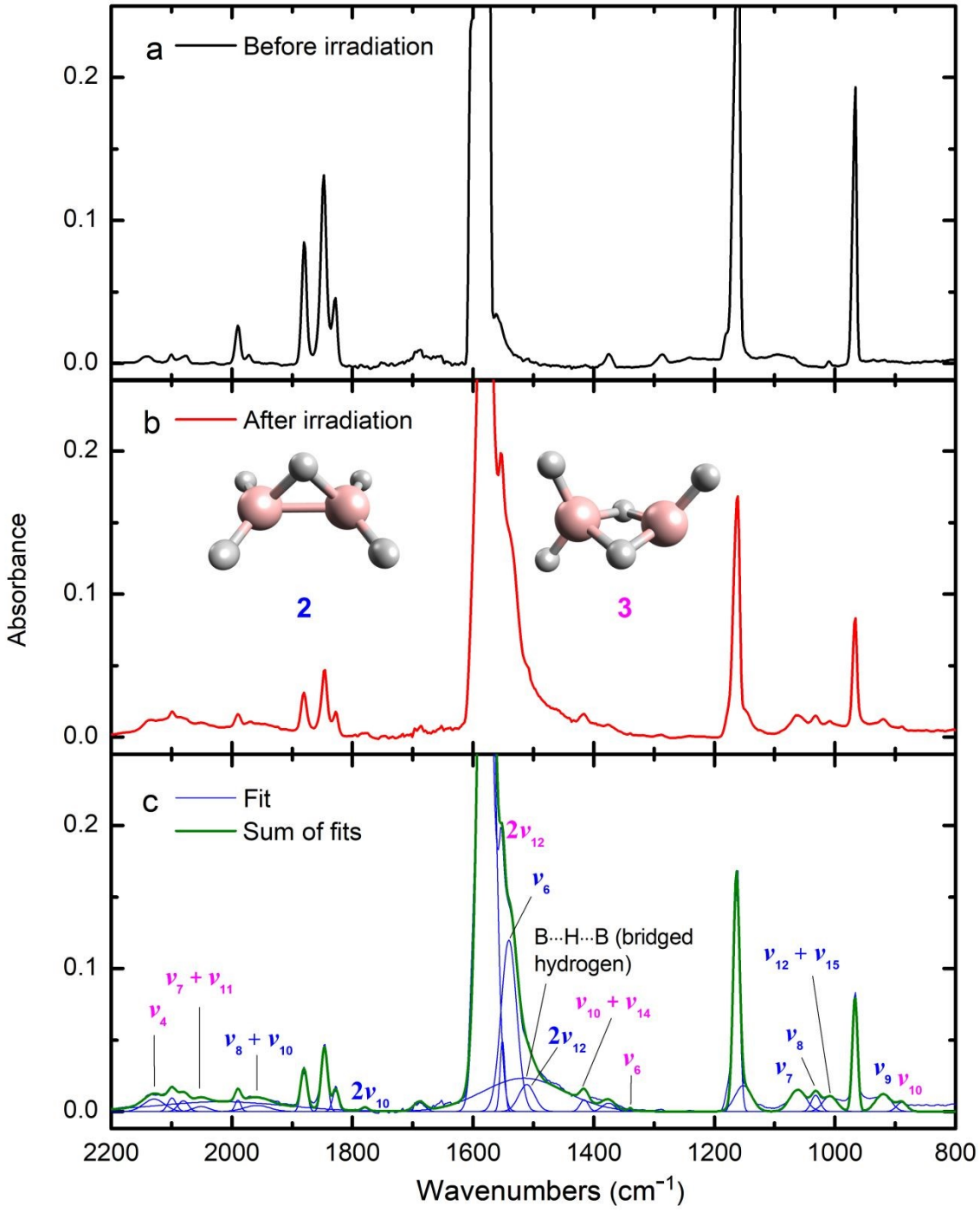

Fig. 2 A magnified view of FTIR spectra of diborane (B_2H_6) ice at 40 K before (a) and after (b) irradiation. The green trace represents the sum of the individual fitted components of the infrared

View Article Online
DOI: 10.1039/D6SC04215E

spectrum after irradiation (c). Detailed assignments are compiled in Table S1. The mono- and dibridged diboranyl (B_2H_5) radicals are labeled in blue and magenta, respectively.

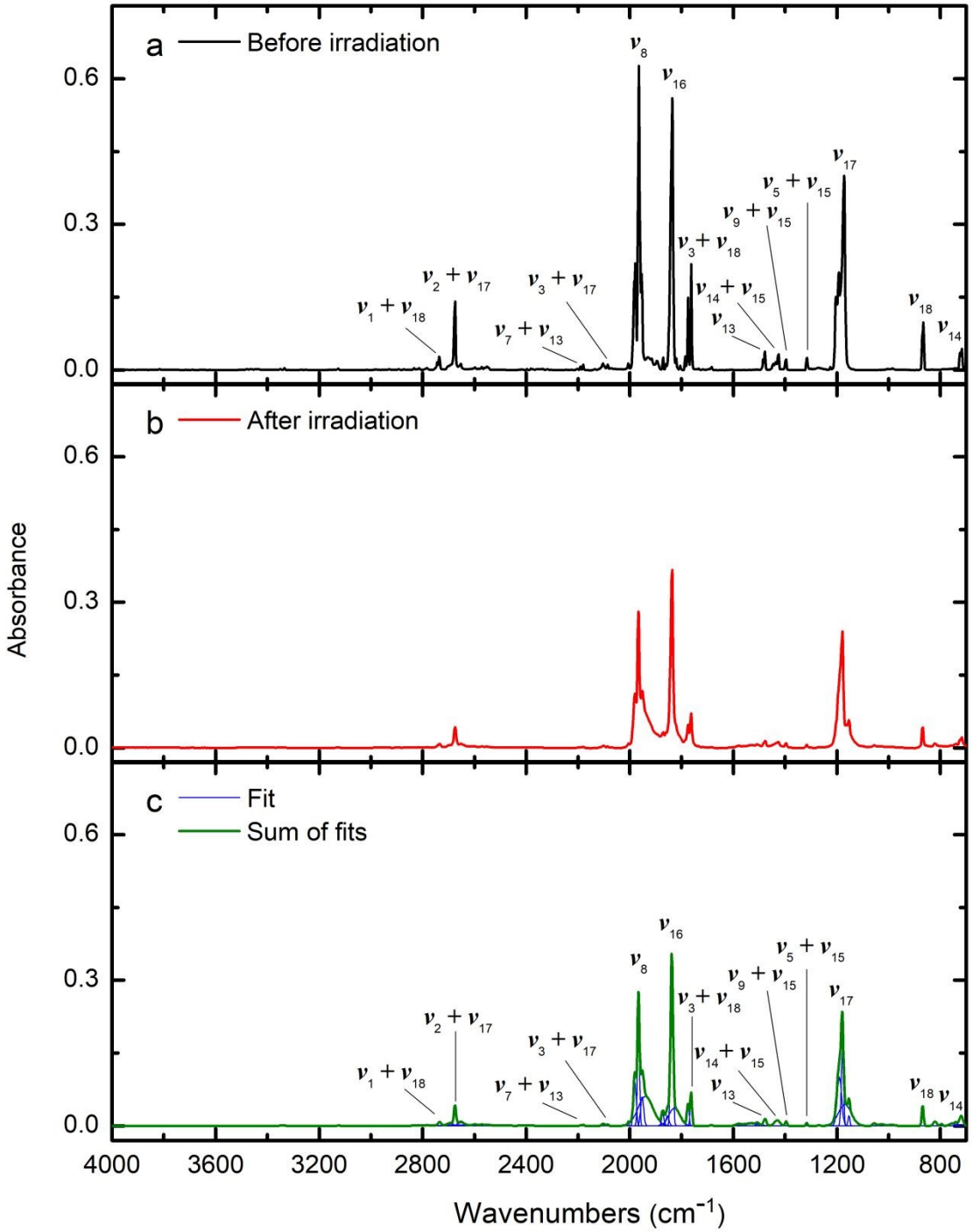

View Article Online
DOI: 10.1039/D6SC04215E

Fig. 3 FTIR spectra of diborane-d_6 (B_2D_6) ice at 40 K before (a) and after (b) irradiation at a current of 116 nA for 120 minutes (a). The green trace represents the sum of the individual fitted components of the infrared spectrum after irradiation (c). Detailed assignments are compiled in Table S2.

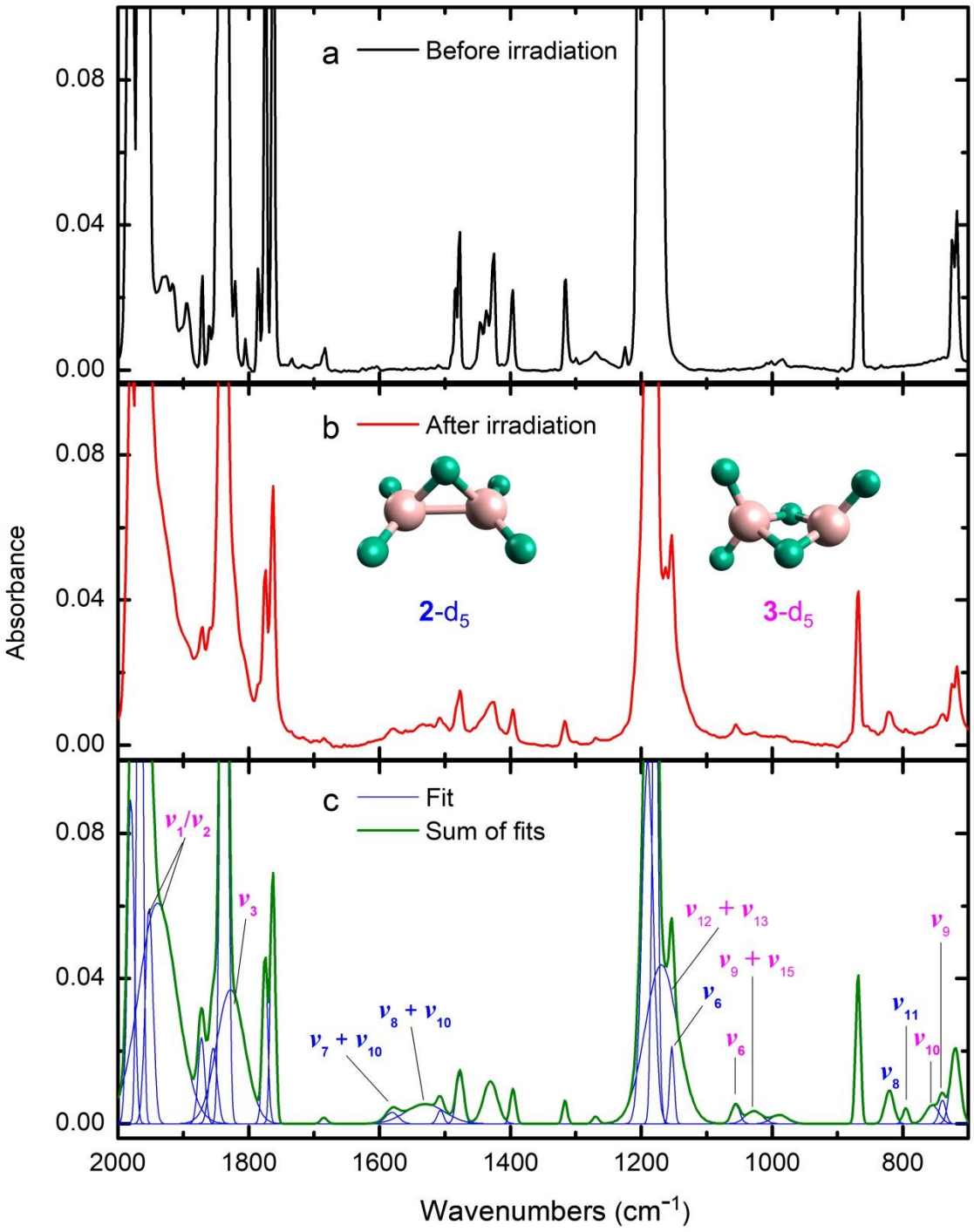

View Article Online
DOI: 10.1039/D6SC04215E

Fig. 4 A magnified view of FTIR spectra of diborane (B_2D_6) ice at 40 K before (a) and after (b) irradiation. The green trace represents the sum of the individual fitted components of the infrared spectrum after irradiation (c). Detailed assignments are compiled in Table S2. The mono- and dibridged diboranyl (B_2D_5) radicals are labeled in blue and magenta, respectively.

B_2H_6 ice (Figs. 1–2, Table S1). The absorption bands at 2501, 1541, 1061, 1032, and 920 cm^{-1} are assigned to the fundamental vibrational modes ν_4, ν_6, ν_7, ν_8, and ν_9 of the monobridged diboranyl radical (**2**), respectively.[13] Additional features at 1958, 1779, 1511, and 1008 cm^{-1} are attributed to combination modes, corresponding to $\nu_8 + \nu_{10}$, $2\nu_{10}$, $2\nu_{12}$, and $\nu_{12} + \nu_{15}$ of isomer **2**. In contrast, the dibridged diboranyl radical (**3**) exhibits absorptions at 2129, 1339, and 889 cm^{-1}, assigned to the fundamental modes ν_4, ν_6, and ν_{10}, respectively, while bands at 2050, 1551, and 1416 cm^{-1} can be assigned to combination bands $\nu_7 + \nu_{11}$, $2\nu_{12}$, and $\nu_{10} + \nu_{14}$.[13] The assignments of both species are further confirmed in irradiated B_2D_6 ice (Figs. 3–4, Table S2). Specifically, the absorptions at 1581, 1530, 1153, 821, and 796 can be assigned to the $\nu_7 + \nu_{10}$, $\nu_8 + \nu_{10}$, ν_6, ν_8, and ν_{11} modes of **2**, respectively.[13] Similarly, absorptions at 1939 and 1952, 1828, 1169, 1056, 1028, 755, and 740 cm^{-1} are attributed to the ν_1 / ν_2, ν_3, $\nu_{12} + \nu_{13}$, ν_6, $\nu_9 + \nu_{15}$, ν_{10}, and ν_9 modes of the dibridged isomer (**3**), respectively.[13] In irradiated B_2H_6 ice, the observed (calculated) bands at 1958 (1969), 1541 (1558), and 1032 (1036) cm^{-1}, assigned to $\nu_8 + \nu_{10}$, ν_6, and ν_8 of radical **2**, respectively, shift upon deuteration to 1530 (1549), 1153 (1122), and 821 (818) cm^{-1} in irradiated B_2D_6 ice. Similarly, the bands at 1339 (1359) and 889 (893) cm^{-1}, attributed to ν_6 and ν_{10} of radical **3**, respectively, shift to 1056 (1049) and 756 (757) cm^{-1} in irradiated B_2D_6 ice.

The temporal evolution of absorption features assigned to **2** and **3** during irradiation of diborane and diborane-d_6 ices is shown in Fig. 5. In B_2H_6 ice, absorptions associated with the monobridged isomer (**2**) exhibit an initial increase in intensity within the first 30 minutes of irradiation, followed by a gradual approach to a plateau. Specifically, the absorptions at 1779 ($2\nu_{10}$), 1032 (ν_8), and 920 (ν_9) cm^{-1} display similar growth trends (Fig. 5a), indicating the concurrent formation of **2**. A similar temporal trend is observed in the B_2D_6 ice, where the corresponding bands at 1581 ($\nu_7 + \nu_{10}$), 1530 ($\nu_8 + \nu_{10}$), and 821 (ν_8) cm^{-1} increase steadily before leveling off (Fig. 5c), consistent with isotopic substitution and thus supporting the assignment. In contrast, the absorptions assigned to the dibridged isomer (**3**) exhibit a different temporal behavior. The absorptions at 1416 (ν_{10} +

View Article Online
DOI: 10.1039/D6SC04215E

ν_{14}) and 889 (ν_{10}) cm^{-1} in irradiated B_2H_6 ice (Fig. 5b), as well as the bands at 1056 (ν_6) and 740 (ν_9) cm^{-1} in irradiated B_2D_6 ice (Fig. 5d) show a delayed onset, followed by a slower and more continuous increase in intensity during irradiation. Notably, the band at 1516 cm^{-1} observed in irradiated B_2H_6 ice is tentatively assigned to the asymmetric in-phase motion of the bridging hydrogen atom within the B···H···B framework of one or more newly formed boranes.[25]

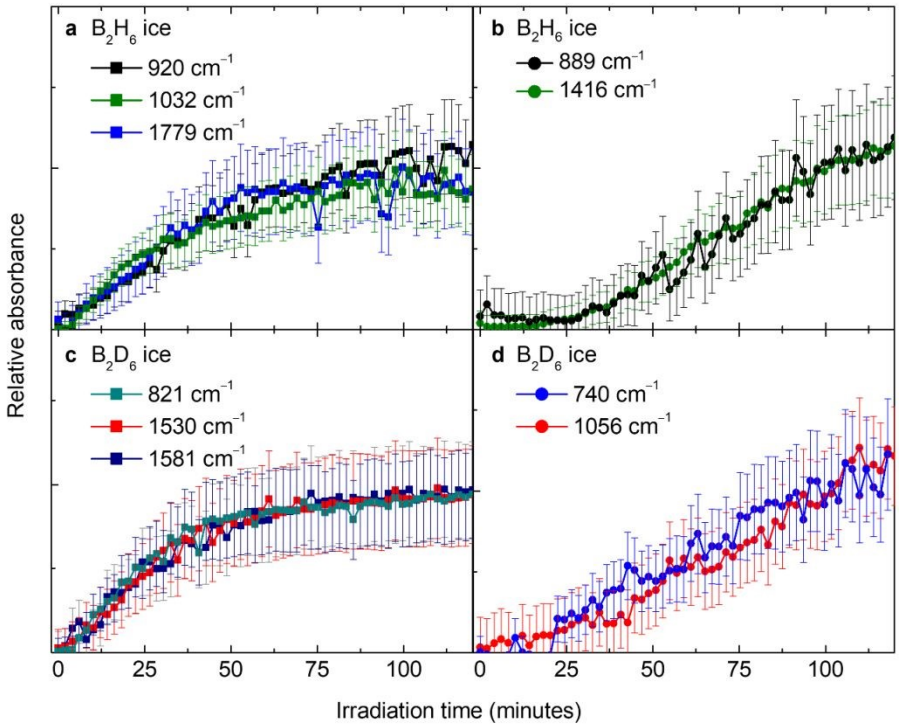

Fig. 5 Temporal evolution of absorption features assigned to monobridged (a, c) and dibridged (b, d) diboranyl radicals in irradiated diborane and diborane-d_6 ices.

View Article Online
DOI: 10.1039/D6SC04215E

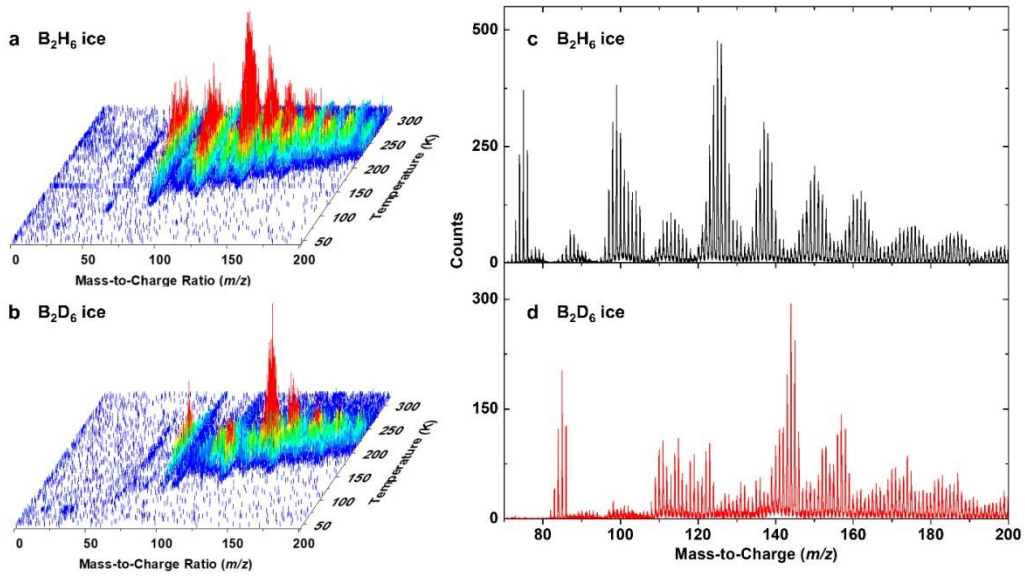

Fig. 6 PI-ReToF-MS mass spectra collected during temperature-programmed desorption (TPD) of electron-irradiated diborane ices at 9.34 eV. Spectra are shown for diborane (a) and diborane-d_6 (b) ices, along with the corresponding integrated ion signals for diborane (c) and diborane-d_6 (d) ices.

The structures of radicals **2** and **3** are shown in Figs. 2 and 4. From a chemical bonding perspective, radical **2** contains four localized B–H σ bonds and one B–B σ bond, together with a delocalized B–H–B bond.[26] Therefore, the radical character is delocalized over the diboron framework rather than localized on a single boron atom. However, due to overlapping absorption features from complex irradiation products, FTIR spectroscopy alone does not allow for the unambiguous identification of individual borane products, indicating that a complementary technique is needed to characterize the formation of complex boranes.

Photoionization Reflectron Time-of-Flight Mass Spectrometry

The photoionization reflectron time-of-flight mass spectrometry (PI-ReToF-MS) technique is utilized to identify complex borane products through their desorption temperatures and isotopic substitution experiments.[27,28] The PI-ReToF mass spectra of the irradiated B_2H_6 and B_2D_6 ices recorded at a photon energy of 9.34 eV during TPD are presented along with the corresponding integrated ion signals in the *m/z* = 70–200 range (Fig. 6). At 9.34 eV, the TPD profile of the ion signal at mass-to-charge ratio (*m/z*) of 76 for the irradiated B_2H_6 ice exhibits a broad sublimation

View Article Online
DOI: 10.1039/D6SC04215E

event spanning 135–290 K, with a maximum centered at 205 K (Fig. 7a). To verify the molecular formula, an additional experiment using fully deuterated B_2D_6 ice was carried out. The TPD profile of *m/z* = 86 for the irradiated B_2D_6 ice shows the same sublimation temperature range and a comparable peak maximum at 202 K, indicating the presence of exactly 10 hydrogen atoms and thereby suggesting the molecular formula as B_6H_{10}. Separate blank experiments in the absence of electron irradiation were performed for both B_2H_6 ice and B_2D_6 ice under otherwise identical experimental conditions (Fig. 7a); no sublimation events were observed, confirming that the above sublimation events are induced by the electron irradiation of diborane ices. Considering the natural isotopic distribution of stable boron ^{10}B to ^{11}B (25.2%), the molecular assignment was further supported by the results obtained from the B_2D_6 ice experiment, which provide better-resolved separation of overlapping mass channels (Fig. 7d). The calculated isotopic distribution of $^{10}B_5{}^{11}BD_{10}$ (*m/z* = 81), $^{10}B_4{}^{11}B_2D_{10}$ (*m/z* = 82), $^{10}B_3{}^{11}B_3D_{10}$ (*m/z* = 83), $^{10}B_2{}^{11}B_4D_{10}$ (*m/z* = 84), $^{10}B^{11}B_5D_{10}$ (*m/z* = 85), and $^{11}B_6D_{10}$ (*m/z* = 86) agrees well with the experimentally observed ion signals of *m/z* = 81–86 in irradiated B_2D_6 ice (Fig. 7b–7c), providing further evidence for the assignment of B_6H_{10}. Because B_6H_{10} can exist in multiple isomers and the adiabatic ionization energy (IE) has only been measured for hexaborane (10) (9.0 ± 0.1 eV) via photoelectron spectroscopy,[29] which agrees well with the calculated value of 8.822 eV.[30] This compound can be photoionized at 9.34 eV; therefore, we tentatively assign the observed signal to hexaborane (10).

Similarly, further boranes including B_6H_{14} (*m/z* = 80), B_7H_{11} (*m/z* = 88), B_8H_{12} (*m/z* = 100), B_8H_{14} (*m/z* = 102), B_8H_{16} (*m/z* = 104), B_8H_{18} (*m/z* = 106), B_9H_{15} (*m/z* = 114), B_9H_{17} (*m/z* = 116), B_9H_{19} (*m/z* = 118), $B_{10}H_{16}$ (*m/z* = 126), $B_{10}H_{18}$ (*m/z* = 128), $B_{10}H_{22}$ (*m/z* = 132), $B_{11}H_{19}$ (*m/z* = 140), $B_{12}H_{20}$ (*m/z* = 152), $B_{12}H_{22}$ (*m/z* = 154), and $B_{12}H_{26}$ (*m/z* = 158) were identified via isotopic distribution analysis from the irradiated B_2D_6 ice (Figs. S3–S18). Among these products, B_9H_{19}, $B_{10}H_{22}$, $B_{11}H_{19}$, $B_{12}H_{22}$, and $B_{12}H_{26}$ are identified for the first time. Notably, the ionization energies of small boranes such as tetraborane (B_4H_{10}; IE = 10.76 ± 0.04 eV) and pentaborane (B_5H_9; IE = 9.90 ± 0.03 eV)[31,32] are higher than 9.34 eV; therefore, they cannot be detected under the present experimental conditions. The IEs of octaborane(12) and decaborane(16) have been measured to be 9.52 ± 0.1 and 10.1 ± 0.2 eV, respectively,[33,34] both exceeding the photon energy of 9.34 eV used in the experiments. Accordingly, the ion signals of *m/z* = 100 ($B_8H_{12}^+$) and 126 ($B_{10}H_{16}^+$) cannot originate from octaborane(12) and decaborane(16), respectively, and are instead tentatively assigned to other isomers with the same molecular formulae. Since each borane composition may

View Article Online
DOI: 10.1039/D6SC04215E

correspond to multiple structural isomers, future studies should focus on isomer-selective identification through combined experimentally determined and theoretically computed adiabatic ionization energies for all relevant isomers. For instance, B_6H_{14} has 48 proposed isomers and its structural assignment may be further complicated by fluxional behavior.[35] The possible structures of several detected boranes are provided in Fig. S19.

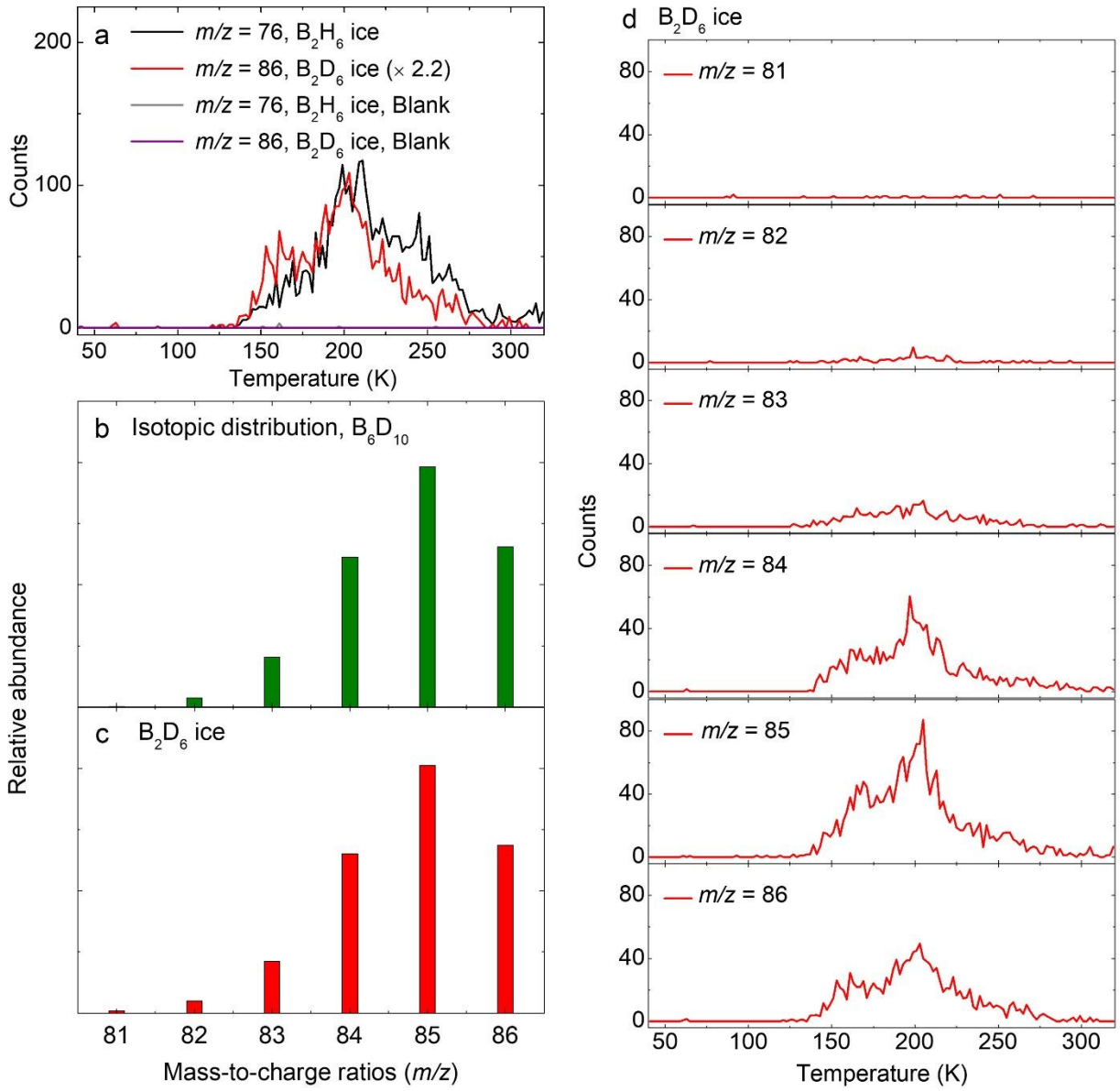

Fig. 7 TPD profiles of m/z = 76 for diborane ice and m/z = 86 for diborane-d_6 ices recorded at a photon energy of 9.34 eV (a). Calculated isotopic distribution of B_6D_{10} (b) compared with

View Article Online
DOI: 10.1039/D6SC04215E

experimental ion signals at *m/z* = 81–86 from irradiated diborane-d_6 ice (c), along with the corresponding TPD profiles (d).

Discussion

Having provided compelling evidence for the formation of monobridged (**2**) and dibridged (**3**) diboranyl radicals, along with complex boranes ranging from B_6H_{10} to $B_{12}H_{26}$, in low-temperature (40 K) diborane (**1**) ices exposed to ionizing radiation in the form of energetic electrons, we now consider their potential formation pathways. We note that the diborane ices were exposed to relatively low irradiation doses, under which the chemistry is expected to be dominated primarily by the decomposition of reactants. Consequently, the abundances of higher boranes are anticipated to remain much lower than those of the initially formed diboranyl radicals. Previous studies of electron-irradiated diborane ices at 10 K revealed that unimolecular decomposition of diborane (**1**) leads to B–H bond cleavage, forming atomic hydrogen (H) and the monobridged radical (**2**) (reaction (1)),[13] which may subsequently yield the dibridged radical (**3**) via isomerization (reaction (2)). However, no definitive evidence for the dibridged B_2H_5 isomer was obtained upon irradiation at 10 K.[13] In contrast, performing the experiments at higher temperature (40 K) may enhance the mobility and reactivity of the monobridged diboranyl radical (**2**), thereby facilitating its isomerization leading to the dibridged isomer (**3**). Reactions (1) and (2) are endoergic by 418 and 19 kJ mol^{-1},[36,37] respectively, calculated at the G3//B3LYP level of theory.[37] The isomerization barrier from **2** to its dibridged isomer (**3**) is calculated to be 36 kJ mol^{-1} at the MP4SDTQ/6-31G*//UHF/6-31G* level of theory.[38]

$$B_2H_6\ (X^1A_g,\ \mathbf{1}) \rightarrow B_2H_5\ (X^2A_1,\ \mathbf{2}) + H, \qquad \Delta H_r^\circ\ (298\ K) = +\ 418\ kJ\ mol^{-1} \qquad (1)$$

$$B_2H_5\ (X^2A_1,\ \mathbf{2}) \rightarrow B_2H_5\ (X^2A',\ \mathbf{3}), \qquad \Delta H_r^\circ\ (298\ K) = +\ 19\ kJ\ mol^{-1} \qquad (2)$$

To probe the kinetic relationships between the diborane decay and product formation, the temporal evolution of the integrated absorbances of B_2H_6 (**1**) and the B_2H_5 radicals (**2** and **3**) were analyzed (Fig. 8). The decay of B_2H_6 as traced by the 1847 cm^{-1} band is accompanied by a rapid rise followed by a plateau for the 1032 cm^{-1} (ν_8) band assigned to **2**, indicating its formation at early stages of irradiation. In contrast, the 889 cm^{-1} (ν_{10}) band attributed to **3** exhibits a delayed onset and a more gradual increase throughout the irradiation period, suggesting a secondary formation process. These distinct temporal behaviors are consistent with the proposed formation pathways,

View Article Online
DOI: 10.1039/D6SC04215E

in which the dibridged isomer (**3**) arises from isomerization of the initially formed monobridged radical (**2**), i.e. a sequential pathway B_2H_6 (**1**) → B_2H_5 (**2**) → B_2H_5 (**3**). In addition, processes including molecular growth to more complex boranes and their fragmentation may contribute to the depletion of B_2H_6. The temporal profiles fit well (Fig. 8) with coupled differential equations using a sequential kinetic reaction scheme (Fig. S20), supporting the formation of diboranyl radicals **2** and **3**. The rate constants (k_1, k_2) of reactions (1) and (2) were determined to be (6.6 ± 1.3) × 10^{-5} s^{-1} and (7.3 ± 1.5) × 10^{-5} s^{-1}, respectively.

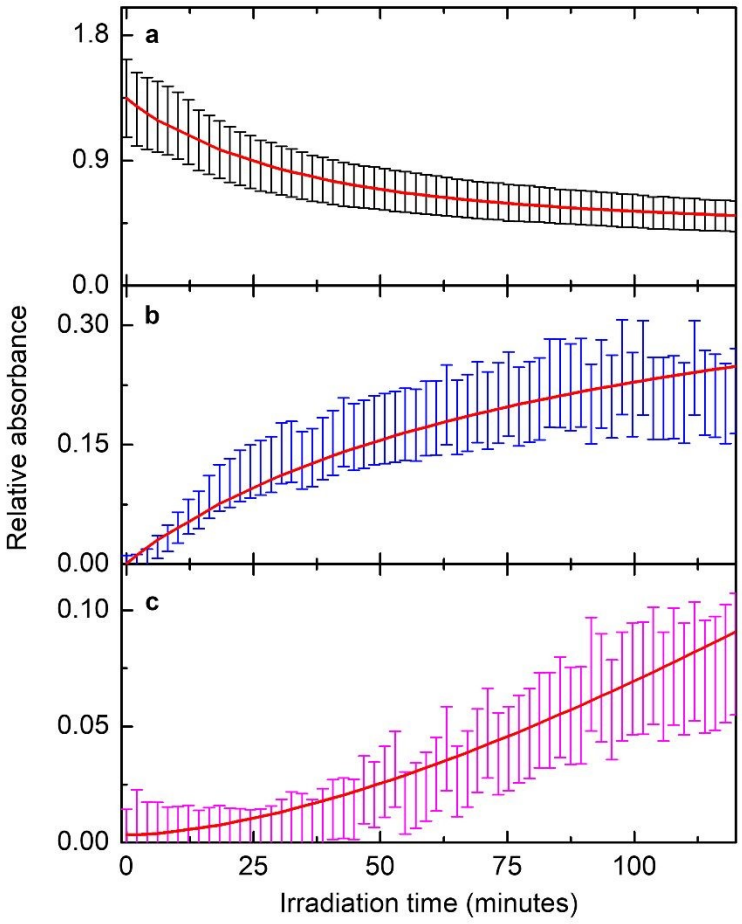

Fig. 8 Temporal evolution of absorption features during irradiation of diborane (B_2H_6) ice along with their corresponding kinetic fits (red curves). (a) Diborane at 1847 cm^{-1}, (b) monobridged diboranyl radical at 1032 cm^{-1}, and (c) dibridged diboranyl radical at 889 cm^{-1}.

Additionally, the proposed formation pathways leading to the detected boranes are presented in Fig. S21. Previous studies demonstrated the synthesis of B_8H_{12} and B_9H_{15} through the reaction of

View Article Online
DOI: 10.1039/D6SC04215E

nonaborane (12) with hydrogen chloride (HCl) in the presence of diborane[39] and by the treatment of KB_9H_{14} with HCl,[40] respectively. Furthermore, B_8H_{16} and $B_{10}H_{18}$ were isolated from the reaction of B_5H_9 with B_2H_6 at elevated temperatures in a flow-quench system.[2] These results suggest that the formation mechanism of complex diboranes such as B_9H_{15} proceeds through borane-addition reactions involving smaller borane precursors.[2,41] Under electron irradiation, the complex boranes observed in the present study are therefore proposed to form via a stepwise boron-insertion mechanism dominated by BH and BH_3 additions coupled with hydrogenation reactions. Starting from smaller species such as B_6H_{10}, borane network can undergo sequential growth toward larger species up to $B_{12}H_{26}$. Specifically, successive BH and BH_3 additions to B_6H_{10} produce $B_{11}H_{19}$ and $B_{12}H_{22}$, which can subsequently convert to $B_{12}H_{26}$ through hydrogenation. The intermediate species such as B_8H_{12}, B_9H_{15}, and $B_{10}H_{16}$ serve as key branching points that either promote further cage expansion to yield $B_{12}H_{26}$ through successive incorporation of BH and BH_3 or lead to increasingly hydrogen-saturated boranes such as B_8H_{18} and $B_{18}H_{22}$ via hydrogenation pathways.

Conclusion and outlook

In conclusion, the hitherto elusive dibridged diboranyl radical (B_2H_5, **3**) as well as the boranes B_9H_{19}, $B_{10}H_{22}$, $B_{11}H_{19}$, $B_{12}H_{22}$, and $B_{12}H_{26}$ have been identified for the first time. These molecules were synthesized in low-temperature diborane and diborane-d_6 ices exposed to energetic electron irradiation at 40 K. The monobridged (**2**) and dibridged (**3**) diboranyl radicals were detected via Fourier transform infrared spectroscopy in the irradiated diborane ices, revealing that radical **2** forms through diborane bond cleavage, followed by isomerization to radical **3**. Complementary tunable vacuum ultraviolet photoionization reflectron time-of-flight mass spectrometry combined with isotopic labeling experiments enabled the identification of boranes ranging from B_6H_{10} to $B_{12}H_{26}$ in the gas phase during temperature-programmed desorption process. The growth of increasingly complex borane species is proposed to proceed via a sequential boron-insertion mechanism dominated by BH and BH_3 addition reactions coupled with hydrogenation steps. Further experiments could focus on the isomer-selective identification of boranes by employing tunable photon energies in combination with their calculated adiabatic ionization energies. These findings establish non-equilibrium chemistry as an efficient pathway toward the synthesis of reactive diboranyl radicals and complex boranes under extreme conditions. The present study

View Article Online
DOI: 10.1039/D6SC04215E

provides fundamental insight into boron chemistry in low-temperature diborane ices, advancing our understanding of the molecular evolution of boron-containing species in extreme environments.

Author contributions

R. I. K. designed the experiments; J. W., J. H. M., C. Z., and A. M. T. carried out the experiments; J. W. analyzed the data with assistance from M. M. and M. N.; J. W. and R. I. K. wrote the manuscript.

Conflict of interest

The authors declare no competing interests.

Data availability

Essential data are provided in the main text and the Supporting Information. Additional data are available from the corresponding author upon reasonable request.

Supplemental Information

Experimental and computational methods, FTIR spectral assignments of diborane ice and diborane-d_6 ice (Figs. S1–S2, Tables S1–S2), formula assignments of mass channels of boranes (Figs. S3–S18), possible structures of several detected boranes (Fig. S19), kinetic reaction scheme (Fig. S20), proposed formation pathways leading to boranes (Fig. S21), and experimental conditions (Table S3).

Acknowledgments

R.I.K. acknowledges support from the U.S. National Science Foundation (NSF), Division of Chemistry (CHEM 2244717).

References

1 A. Stock and C. Massenez, *Ber. Dtsch. Chem. Ges.*, 1912, **45**, 3539-3568.
2 J. Dobson, R. Maruca and R. Schaeffer, *Inorg. Chem.*, 1970, **9**, 2161-2166.
3 M.-Y. Lin, T.-P. Huang, C.-H. Chin and Y.-J. Wu, *J. Chem. Phys.*, 2018, **148**.
4 E. Bernhardt, A. Drichel, M. Krnel, E. Svanidze and A. Slabon, *Inorg. Chem.*, 2024, **63**, 5414-5422.

View Article Online
DOI: 10.1039/D6SC04215E

5 Y. Jing, X. Wang, H. Han, X.-R. Liu, X.-C. Yu, X.-M. Chen, D. Wei, L.-S. Wang and X. Chen, *Science China Chemistry*, 2024, **67**, 876-881.
6 B. Ruščić, M. Schwarz and J. Berkowitz, *J. Chem. Phys.*, 1989, **91**, 4183-4188.
7 N. Balucani, F. Zhang and R. I. Kaiser, *Chem. Rev.*, 2010, **110**, 5107-5127.
8 Y.-C. Peng, S.-L. Chou, J.-I. Lo, M.-Y. Lin, H.-C. Lu, B.-M. Cheng and J. F. Ogilvie, *J. Phys. Chem. A*, 2016, **120**, 5562-5572.
9 M.-C. Liu, H.-F. Chen, W.-J. Huang, C.-H. Chin, S.-C. Chen, T.-P. Huang and Y.-J. Wu, *J. Chem. Phys.*, 2016, **145**.
10 L. A. Curtiss and J. A. Pople, *J. Chem. Phys.*, 1989, **91**, 4189-4192.
11 S. Yan-Bo, W. Di, L. I. Ze-Sheng, H. Xu-Ri and S. Chia-Chung, *Chem. J. Chin. Univ.* , 2002, **23**, 1727-1730.
12 S. X. Tian, *J. Phys. Chem. A*, 2005, **109**, 5471-5480.
13 J. G. Longenecker, A. M. Mebel and R. I. Kaiser, *Inorg. Chem.*, 2007, **46**, 5739-5743.
14 P. D. Pancharatna, S. H. Dar and M. M. Balakrishnarajan, in *Comprehensive Inorganic Chemistry III (Third Edition)*, eds. J. Reedijk and K. R. Poeppelmeier, Elsevier, Oxford, 2023, DOI: https://doi.org/10.1016/B978-0-12-823144-9.00118-7, pp. 26-50.
15 H. C. Longuet-Higgins and M. D. V. Roberts, *Proc. R. Soc. A*, 1954, **224**, 336-347.
16 W. N. Lipscomb and I. R. Epstein, *Inorg. Chem.*, 1971, **10**, 1921-1928.
17 W. N. Lipscomb, *Science*, 1977, **196**, 1047-1055.
18 D. Sun, X. Song, L. Liu, C. Song, H. Liu, Q. Li, K. Butler, C. Xie, Z. Zhang and Y. Xie, *J. Phys. Chem. Lett.*, 2024, **15**, 9668-9676.
19 J. C. Howk, K. R. Sembach and B. D. Savage, *Astrophys. J.*, 2000, **543**, 278.
20 A. M. Ritchey, S. R. Federman, Y. Sheffer and D. L. Lambert, *Astrophys. J.*, 2011, **728**, 70.
21 K. Lodders, *Astrophys. J.*, 2003, **591**, 1220.
22 C.-L. Yu and S. H. Bauer, *J. Phys. Chem. Ref. Data*, 1998, **27**, 807-835.
23 E. C. Neeve, S. J. Geier, I. A. I. Mkhalid, S. A. Westcott and T. B. Marder, *Chem. Rev.*, 2016, **116**, 9091-9161.
24 J. L. Duncan, D. C. McKean, I. Torto and G. D. Nivellini, *J. Mol. Spectrosc.*, 1981, **85**, 16-39.
25 G. Socrates, *Infrared and raman characteristic group frequencies: Tables and charts*, John Wiley & Sons, Ltd., New York, 3rd edn., 2004.
26 A. S. Pozdeev and I. A. Popov, *Chem. Phys. Rev.*, 2024, **5**, 011401.
27 A. M. Turner and R. I. Kaiser, *Acc. Chem. Res.*, 2020, **53**, 2791-2805.
28 J. Wang, J. H. Marks, A. M. Turner, A. A. Nikolayev, V. Azyazov, A. M. Mebel and R. I. Kaiser, *Phys. Chem. Chem. Phys.*, 2023, **25**, 936-953.
29 J. A. Ulman and T. P. Fehlner, *J. Am. Chem. Soc.*, 1978, **100**, 449-456.
30 S. X. Tian, *J. Phys. Chem. A*, 2005, **109**, 6580-6586.
31 P. J. Linstrom and W. G. Mallard, *NIST Chemistry webBook, NIST standard reference database number 69*, 2013, DOI: http://webbook.nist.gov/.
32 D. R. Lloyd, N. Lynaugh, P. J. Roberts and M. F. Guest, 1975, **71**, 1382-1394.
33 F. E. Stafford, S. J. Steck, G. A. Pressley, Jr., J. Dobson and R. Schaeffer, *Inorg. Chem.*, 1970, **9**, 2452-2457.
34 L. H. Hall, V. V. Subbanna and W. S. Koski, *J. Am. Chem. Soc.*, 1964, **86**, 3969-3973.
35 E. Fontain, *Heteroatom Chemistry*, 1994, **5**, 61-64.
36 B. Ruscic and H. Bross, *Active Thermochemical Tables (ATcT) values based on ver. 1.220 of the Thermochemical Network*, Argonne National Laboratory, 2025.

View Article Online
DOI: 10.1039/D6SC04215E

37 Y. Zeng, K. Su, J. Deng, T. Wang, Q. Zeng, L. Cheng and L. Zhang, *J. Mol. Struct. (Theochem)*, 2008, **861**, 103-116.
38 M. Trachtman, C. W. Bock, H. Niki and G. J. Mains, *Struct. Chem.*, 1990, **1**, 171-178.
39 D. B. MacLean, J. D. Odom and R. Schaeffer, *Inorg. Chem.*, 1968, **7**, 408-411.
40 J. Dobson, P. C. Keller and R. Schaeffer, *J. Am. Chem. Soc.*, 1965, **87**, 3522-3523.
41 R. Maruca, J. D. Odom and R. Schaeffer, *Inorg. Chem.*, 1968, **7**, 412-418.

View Article Online
DOI: 10.1039/D6SC04215E

Data availability

Essential data are provided in the main text and the Supporting Information. Additional data are available from the corresponding author upon reasonable request.